



Shock-melted material in the Krymka LL3.1 chondrite: Behavior of the opaque minerals

Vira P. SEMENENKO^{1*} and Claude PERRON²

¹Institute of Environmental Geochemistry, National Academy of Sciences of Ukraine, Kyiv-142, 03180 Ukraine

²Laboratoire d'Etude de la Matière Extraterrestre, Muséum National d'Histoire Naturelle and CNRS, 75005 Paris, France

*Corresponding author. E-mail: virasem@i.com.ua

(Received 04 September 2004; revision accepted 22 December 2004)

Abstract—Six large millimeter- to centimeter-size regions of one specimen of the Krymka LL3.1 ordinary chondrite show evidence of having been completely or nearly completely shock-melted in situ, a phenomenon rarely observed in primitive chondrites. The shock pressure, nominally in the range of 75–90 GPa, could only have been 30–35 GPa in a porous material like fine-grained matrix. The melted regions have an igneous texture and their silicates are zoned and unequilibrated. Large metal-troilite intergrowths formed in these regions. The metal has a nickel content corresponding to martensite and the troilite contains up to 4.2 wt% nickel. Melting must have been very short and cooling very fast (>100 °C/h at high temperature). The metal contains up to 0.7 wt% phosphorus. Abundant chromite crystals and sodium-iron phosphate glass globules are found in troilite. The differences in composition between the opaque phases found in the melted regions and those generally observed in unmetamorphosed chondrules are assigned to melting under closed system conditions. Surprisingly high Co concentrations (up to 13 wt%) were found in some metal grains in or at the periphery of melted regions. They likely resulted from sulfurization of metal by sulfur vapor produced during the shock. After solidification, at least one other shock led to mechanical effects in the melted regions.

INTRODUCTION

Shock metamorphism of various intensities has affected all kinds of meteorites, but among ordinary chondrites, the most severe shock effects are observed essentially only in equilibrated chondrites, being rare in unequilibrated chondrites (Stöffler et al. 1991).

The Krymka (LL3.1) chondrite, along with Semarkona and Bishunpur, is held to be among the three most primitive ordinary chondrite falls. It has been classified as S3 (weakly shocked) by Stöffler et al. (1991), which corresponds to shock pressures in the range of 5–20 GPa. Examination of many individual Krymka specimens from the Ukrainian meteorite collection by Semenenko et al. (1987) revealed that some specimens do not exhibit any evidence of shock metamorphism, while others contain shock effects such as planar fractures and mosaicism, and, in some cases, recrystallization of olivine, undulatory and mosaic extinction of pyroxene and troilite, lamellar sculpture of the surface of kamacite grains, secondary troilite, indicative of pressures in

the range of 25–45 GPa (assuming nonporous material), and post-shock temperature generally not higher than 500 °C (presence of type IV plessite) with local excursions to 950 °C (melting of troilite-metal eutectic). In addition, Krymka contains many xenoliths, some of which are made of exotic materials (Semenenko and Girich 1995, 1996, 1998, 2001; Semenenko et al. 2001, 2004).

Krymka thus offers the opportunity to study shock effects of various intensities in a low-metamorphic-grade chondrite. In addition, because of the accepted primitive character of this meteorite, it is important to determine to what extent shocks may have affected the properties of its materials. Taking advantage of the large number of Krymka specimens present in the collection of the Museum of Natural History at the National Academy of Sciences of Ukraine, Kyiv, we looked for strong shock effects in this meteorite. Here we report on a mineralogical study of large, completely shock-melted regions in one Krymka specimen, focusing on the opaque phases, Fe-Ni metal, and troilite. Preliminary results have been presented by Semenenko and Perron (1995, 1996).

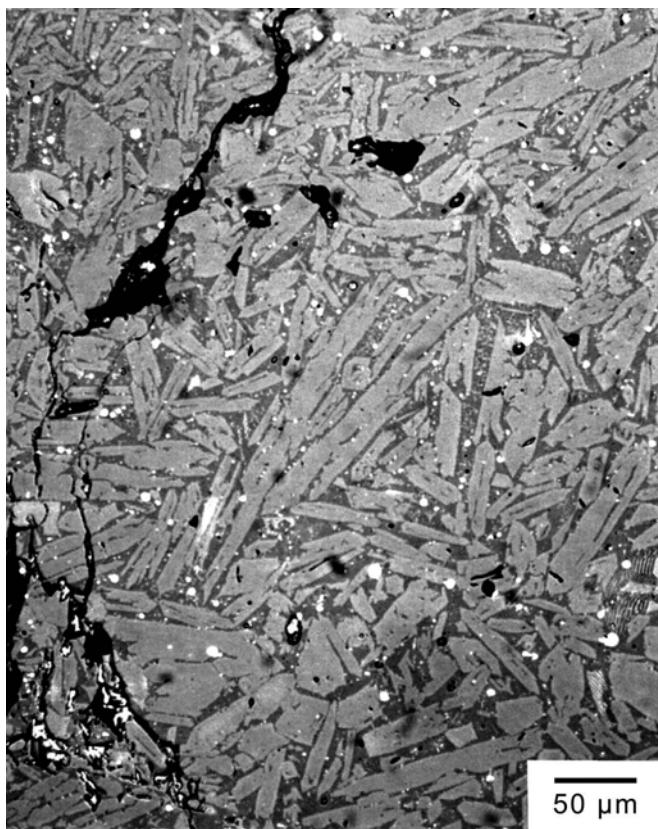


Fig. 1. Reflected light photomicrograph of part of a shock-melted region in the Krymka chondrite. Silicate crystals (olivine and minor pyroxene) are light gray, mesostasis is darker gray. Notice the skeletal morphology of most olivines. Metal globules (white) are dispersed within the mesostasis. The black zones are cracks and holes. Scale bar is 50 μm .

SAMPLES AND INSTRUMENTATION

Six light-colored regions composed of crystalline materials devoid of chondrules were found on a fracture surface of Krymka specimen #1290/29 (140 g) of the Kyiv collection. It should be noted that xenoliths containing graphite have also been found in this very specimen (Semenenko et al. 2004). Polished mounts were prepared with a total area of 14 cm^2 , out of which the light-colored regions represented 3 cm^2 . Although great care was taken in their preparation and polishing as the light-colored material is highly friable, some plucking could not be avoided.

The polished sections were observed with optical microscopes in reflected light and with a JEOL JSM-840A scanning electron microscope (SEM). Mineral compositions were determined in Paris using a Cameca Camebax electron microprobe, operated at an accelerating voltage of 15 kV and a beam current of 10 nA for silicates and 40 nA for metallic phases. After etching in nital, metal was analyzed in Kyiv with a Jeol JCXA-733 electron microprobe, with the same operating conditions. Well-documented natural and synthetic

standards were used, including pure Fe, Ni, and Co for analysis of metal. The energy-dispersive X-ray spectrometer (EDS, Link AN 10000) of the SEM was used for analysis of the smallest grains (phosphates, chromites, Fe-Ni).

Raman spectra of a few inclusions in troilite and of standard minerals were recorded with a Dilor XY (LADIR, Thiais) or a Jobin-Yvon Labram HR800 (ENS, Lyon) Raman microprobe. The 514.5 nm line of an Ar-ion laser or the 632.2 nm line of a He-Ne laser was focused on the sample surface on a spot of approximately 1 μm through the 100 \times objective of an Olympus optical microscope, which also collected the Raman light. After passing through a double monochromator, the Raman light was detected on a cooled CCD.

RESULTS

The light-colored regions have elongated shapes, irregular outlines, and diffuse boundaries. In polished sections, their apparent lengths vary from 2 to 15 μm . They consist of two parts with different textures, the core and the rim, which we shall call the melted region and the transition zone, respectively.

Melted Regions

The melted regions have an igneous texture reminiscent of that of porphyritic chondrules (Fig. 1). They consist of coarse idiomorphic (up to 50 \times 50 μm^2) or skeletal (up to 200 \times 20 μm^2) crystals of olivine, rare Ca-poor pyroxene (up to 120 \times 20 μm^2), and a few large grains of metal-troilite intergrowths (up to 1.5 \times 2 mm^2), all set in a cryptocrystalline mesostasis, apparently consisting of submicroscopic pyroxene, olivine, and plagioclase.

The olivine composition varies both from grain to grain and within grains (Table 1). The range of variation (Fa_{10-28}) is similar for olivine from different melted regions and is independent of the crystal morphology. Figure 2 compares the Fa content distribution in the melted regions to that in the Krymka host (Dodd et al. 1967). A few olivine crystals are included inside the metal-troilite mixtures. These have a higher Fa content (Fa_{35-39}).

Most olivine crystals are normally zoned, with FeO and CaO increasing from core to rim (Fig. 3), as is the case for olivines in Krymka porphyritic chondrules (Radomsky and Hewins 1990). MnO and Cr_2O_3 are positively correlated with the Fa content. Two grains with reverse FeO zoning were found: one that was euhedral and in the mesostasis, and one that was rounded in shape and was within a metal-troilite mixture. These grains differ in composition from each other. The former has a rim enriched in CaO and Cr_2O_3 , while in the latter, the reverse is observed (Fig. 3).

Pyroxene crystals have a lamellar shape. With the exception of only four grains, these crystals are so thin that

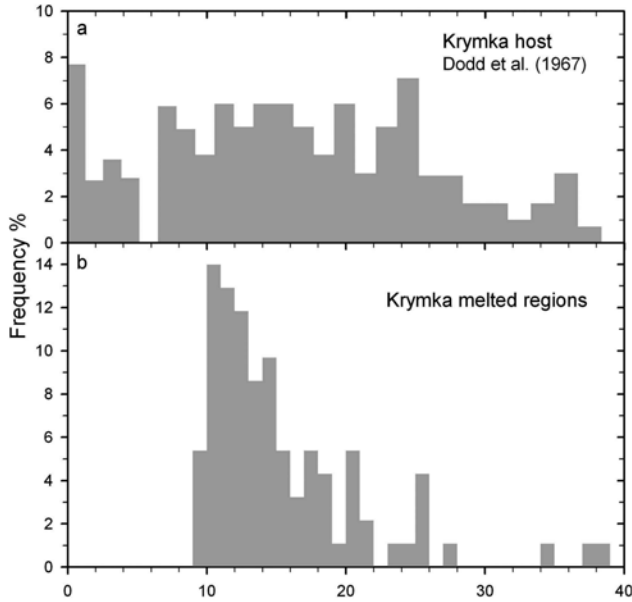


Fig. 2. Fa content distribution in Krymka olivine: a) in the host (103 crystals), after Dodd et al. (1967) (Fe wt% was changed to Fa assuming stoichiometry); b) in shock-melted regions (93 crystals). The three crystals with the highest Fa content in (b) are located within a metal-troilite intergrowth.

their composition could not be determined. This composition appears somewhat variable (Table 1). The composition of the mesostasis varies over a wide range, both between the different regions and within them (Table 1).

The metal-troilite intergrowths are arranged on the periphery of the melted regions. They have a rounded or irregular shape and a dendritic or cellular structure (Fig. 4). Metal dendrites and cells in troilite are smaller than $10 \times 100 \mu\text{m}^2$ and $40 \times 40 \mu\text{m}^2$, respectively.

Iron-nickel cells and dendrites are zoned, consisting of a core whose Ni content lies in the range of 11.5–19 wt% (but see below) and an Ni-rich rim. On the basis of their composition, the cores must be made of martensite, but no clear martensitic structure is visible after etching in nital, which may result from the small size of the metal cells. The rims are so narrow ($\sim 1 \mu\text{m}$) that their composition is difficult to determine precisely with the electron microprobe. The highest value obtained is 38 wt% Ni, but the real value is certainly higher than that. Cobalt is also detected in all metal grains and phosphorus is detected in most of them. Si was found to be below the detection limit ($<0.03 \text{ wt}\%$) in all cases and Cr to be below the detection limit in most cases. Ni, P, and Co concentrations are given in Table 2 and Figs. 5 and 6. Apart from one notable exception, the distribution of Co is almost flat at 0.83–0.96 wt% (Fig. 5), while the concentration of P is variable (Fig. 6). The exception is a grain whose Co content varies from 1.8 to 5 wt% and in which P is below detection limit. Another metal cell in the same metal-troilite

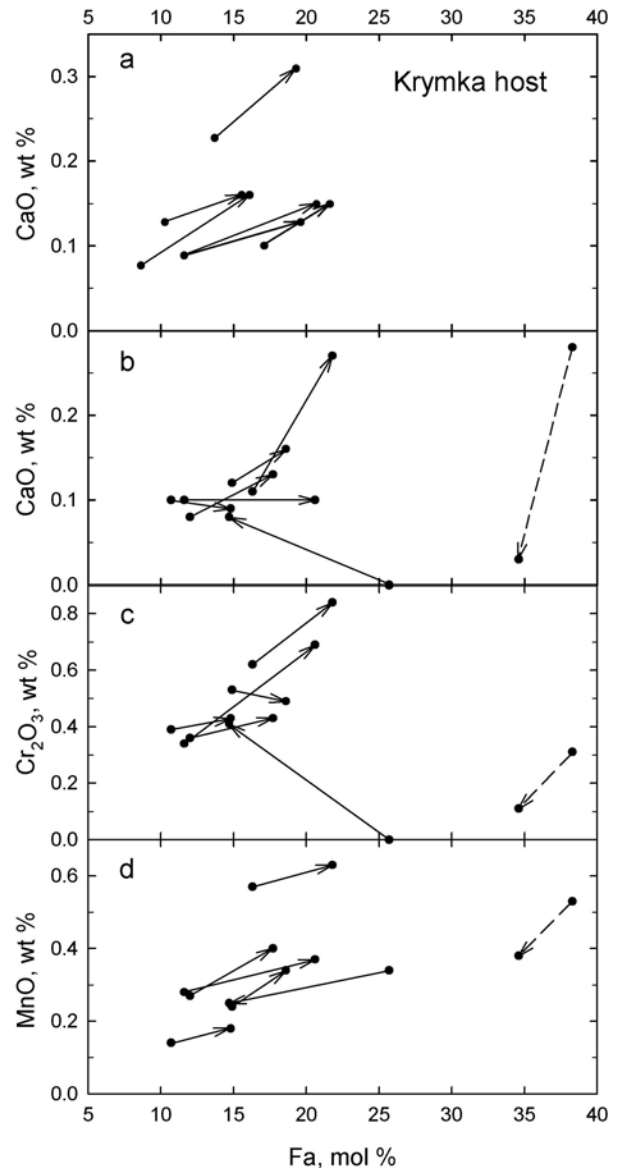


Fig. 3. Olivine zoning trends (values measured at the center and edge of each crystal are joined by an arrow pointing to the edge value): a) CaO versus Fa in Krymka type II porphyritic olivine chondrules (Radomsky and Hewins 1990); b) CaO, c) Cr_2O_3 , d) MnO versus Fa in the shock-melted regions. Most olivine crystals are normally zoned with Fa, CaO, Cr_2O_3 , and MnO increasing from core to edge. One of the two crystals with reverse Fa zoning (dashed line) is located in a metal-troilite intergrowth.

intergrowth has 1.2 wt% Co, which is slightly above average, also without P. Nickel content in these two cells is “normal” (within the range 13.3–17.1 wt%). Fine Ni-rich cells (30.7–51.3 wt% Ni) with sizes less than $4 \times 4 \mu\text{m}^2$ are located on the periphery of some metal-troilite mixtures.

The detailed mineralogy and composition of the metal depend on the melted region where it is located. We identify two types of metal-troilite mixtures. The structure of the first

Table 1. Electron microprobe analyses (wt%) of silicates, mesostasis and chromite in Krymka melted regions.^{a, b}

	Olivine in Mesostasis (85)		Olivine in metal-troilite (3)		Pyroxene (4)		Mesostasis (17)		Chromite in type 1 (21)		Chromite in type 2 (4)	
	range	mean	range	mean	range	mean	range	mean	range	mean	range	mean
SiO ₂	36.4–40.6	39.3	34.9–36.3	35.5	52.7–54.5	53.8	46.7–75.1	58.3	n.d. ^c –0.35	0.09	n.d.–0.16	0.10
TiO ₂	n.d.–0.08	<0.04	n.d.–0.09	<0.04	0.09–0.19	0.13	0.14–0.46	0.34	n.d.–0.22	0.10	n.d.–0.11	0.06
Al ₂ O ₃	n.d.–0.16	<0.04	n.d.–0.09	<0.04	0.42–0.92	0.61	2.66–12.9	6.85	n.d.	<0.04	n.d.	<0.04
Cr ₂ O ₃	n.d.–0.86	0.42	0.11–0.31	0.23	1.50–2.00	1.79	n.d.–1.78	0.58	62.0–65.7	63.8	61.6–62.2	62.0
V ₂ O ₃	n.d.	<0.05	n.d.	<0.05	n.d.	<0.05	n.d.	<0.05	0.24–0.91	0.56	0.34–0.62	0.47
Fe ₂ O ₃ ^d									1.18–5.04	2.88	4.28–5.10	4.54
FeO	9.39–26.7	14.2	30.2–34.0	32.2	12.8–13.5	13.1	3.62–20.7	15.6	30.4–31.2	30.9	30.0–30.9	30.4
MnO	0.14–0.87	0.31	0.38–0.53	0.46	0.71–0.98	0.82	0.18–0.83	0.45	0.36–0.77	0.55	0.42–0.63	0.52
MgO	36.0–50.7	45.9	29.6–32.3	30.8	24.1–27.9	26.0	0.93–28.3	9.40	n.d.–0.40	0.09	n.d.–0.54	0.32
CaO	n.d.–0.28	0.12	n.d.–0.28	0.12	1.92–4.83	3.27	0.68–9.56	5.34	n.d.	<0.03	n.d.–0.05	<0.03
Na ₂ O	n.d.–0.07	<0.04	n.d.–0.07	0.05	n.d.–0.34	0.16	0.31–4.33	1.33	n.d.–0.08	<0.04	n.d.–0.06	<0.04
K ₂ O	n.d.–0.05	<0.03	n.d.	<0.03	n.d.–0.05	<0.03	0.18–1.47	0.44	n.d.	<0.03	n.d.	<0.03
P ₂ O ₅	n.d.–0.20	<0.05	0.14–0.90	0.44	n.d.–0.12	0.06	n.d.–1.65	0.36	n.d.–0.08	<0.05	n.d.–0.24	0.08
Total		100.4		99.8		99.9		99.1		99.1		98.5
Fa	9.5–27.7	15.2	34.6–39.0	37.3								
En					68.1–75.6	71.8						
Fs					20.6–22.8	21.6						
Wo					3.7–9.8	6.5						

^aThe number of analyses is given in parentheses.

^bAll chromites are in metal-troilite intergrowths.

^cn.d. = not detected; the detection limits are given in the “mean” columns, when applicable.

^dCalculated.

Table 2. Electron microprobe analyses (wt%) of metal and troilite in Krymka melted regions.^a

	Low-Ni metal (75)		High-Ni metal (9)		Troilite (20)	
	range	mean	range	mean	range	mean
Fe	78.9–88.2	84.5	47.3–78.5	64.5	58.1–62.8	61.3
Ni	11.5–19.0	14.2	19.9–51.3	34.1	0.05–4.18	1.10
Co	0.83–5.03	1.08 ^b	0.63–1.01	0.89	0.08–0.25	0.16
Cu	n.d. ^c –0.07	<0.05	n.d.–0.17	0.07	n.d.–0.20	0.08
Cr	n.d.–0.12	<0.02	n.d.–0.03	<0.02	n.d.–0.08	0.03
P	n.d.–0.72	0.40	n.d.–0.61	0.20	n.d.–0.93	0.07
S	n.d.–2.07	0.14	n.d.–0.70	0.30	35.9–39.7	38.0
Total		100.3		100.1		100.7

^aThe number of analyses is given in parentheses.

^b0.93 when not taking into account 5 analyses of 2 Co-rich grains.

^cn.d. = not detected; the detection limits are given in the “mean” columns, when applicable.

one (Fig. 7a) is similar to that of metal-troilite intergrowths in the Ramsdorf chondrite, which experienced intensive shock metamorphism (Begemann and Wlotzka 1969). The composition of the metal cores (obtained before etching) is within 11.5–15.0 wt% Ni and 0.19–0.70 wt% P. A positive Ni-P correlation can clearly be seen (Fig. 6a). At higher values of Ni content, near the edge, the P content decreases with increasing Ni, reaching ~0.1 wt% P for the highest values of Ni content. P is also low in the small Ni-rich cells and even undetectable in the most Ni-rich ones (51.3 wt% Ni). After etching, heterogeneously distributed tiny holes (<1 μm in size) appear on the metal surface. Most are rounded, but some exhibit a rectangular shape similar to rhabdites found in iron meteorites. We conclude that the metal probably contains microinclusions of Fe-Ni phosphide (schreibersite), which are lost during etching. The etched metal has a rather uniform composition with 11.2–12.6 wt% Ni and 0.19–0.43 wt% P. The latter is probably in solid solution. Troilite in these mixtures has variable amounts of nickel, with most values in the range 0.6–1.2 wt% and the highest concentration around 4.2 wt% Ni (Table 2). It also contains up to 0.25 wt% Co. Included in the troilite are coarse ($\leq 25 \times 15 \mu\text{m}^2$) euhedral crystals of chromite (Fig. 8) and fine ($\leq 2 \mu\text{m}$) globular inclusions, probably phosphates. The chromite crystals have variable compositions (Table 1) and lower concentrations of Al_2O_3 , MgO , and TiO_2 than those from the Krymka host (Bunch et al. 1967). The largest crystal of chromite is apparently zoned with Cr_2O_3 decreasing from core to rim from 65.2 to 62.4 wt%.

The second type of metal-troilite mixtures (Fig. 7b) differs from the first one by the following features:

1. thin, contorted Ni-rich areas in the metal, with a maximum measured Ni content of 28 wt% (obtained by EDS after etching; here also the real value must be higher than that); the Ni and P contents measured with the electron microprobe before etching vary in the cores within the ranges of 12.5–19.0 and 0–0.7 wt%, respectively; the P-Ni correlation seen for the metal of the first type is present below 14 wt% Ni, but breaks down above this value, the P content scattering between 0 and 0.7 wt% (Fig. 6b).
2. lower content and smaller sizes of chromite crystals (≤ 10 – $15 \mu\text{m}$) within troilite and higher (calculated) concentrations of Fe_2O_3 in chromite. The largest chromites are surrounded by a thin rim of phosphate.
3. presence in troilite of coarse phosphate globules (up to ~20 μm in diameter) containing microcrystals of chromite ($\leq 1 \mu\text{m}$, Fig. 9). One of the phosphate globules preserves clear evidence of shear deformation (Fig. 10).

The measured composition of the phosphates is variable, with varying amounts of Cr (up to 15 wt% Cr_2O_3), probably due to the chromite inclusions, and also of Si (up to 24 wt% SiO_2) and Mg (up to 12.7 wt% MgO), probably due to mixing with silicate. Totals are systematically low. Keeping only the

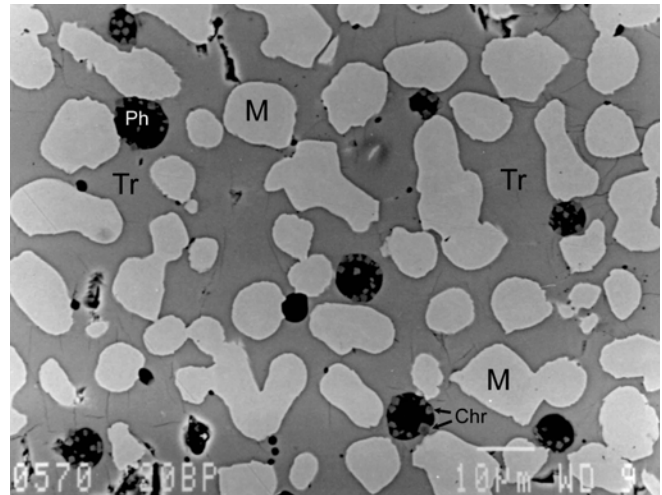


Fig. 4. Backscattered electron (BSE) image of a metal-troilite intergrowth in a shock-melted region. M = metal; Tr = troilite. Black round areas in troilite are phosphate globules (Ph). Most globules contain euhedral chromite microcrystals (Chr). Scale bar is 10 μm .

analyses with the lowest amounts of Cr (<0.6 wt% Cr_2O_3) and Si (<0.2 wt% SiO_2) gives a composition for the phosphate of (in wt%) 7–11 Na_2O , 0.5 K_2O , 40–50 FeO , 0.45 MnO , 37–40 P_2O_5 , <0.2 MgO , <0.2 SiO_2 , and <0.2 CaO . This composition is somewhat Na-poor compared to the sodium-iron phosphate maricite (FeNaPO_4 , 17.8 Na_2O , 41.3 FeO , and 40.8 P_2O_5).

Raman spectra of globules (Fig. 11a) show broad bands in the region of 950–1100 cm^{-1} , which is where phosphate crystals generally have their characteristic bands. This is true particularly for maricite crystals (Mostefaoui 1996), as shown by the spectra obtained from two maricite grains from the Bishunpur chondrite (Fig. 11b). However, the broad bands obtained from the Krymka globules indicate that in this case the phosphate is not crystallized but glassy. Some of the spectra also display broad bands in the 500–700 cm^{-1} region (top spectrum in Fig. 11a), which is typical of silicate glasses. This is consistent with the chemical analyses that show the frequent presence of Si in the globules, as mentioned above. In particular, the lower frequency part of the top spectrum in Fig. 11a is very similar to a spectrum of obsidian (Fig. 11c in Montagnac 2004). Alternatively, the peak near 670 cm^{-1} in the top spectrum of Fig. 11a may be due to the small chromites present in most globules (compare to the bottom spectrum in Fig. 11c). This is supported by the absence of such a peak in the bottom spectrum of Fig. 11a corresponding to one of the rare globules without visible chromite inclusions. The fact that the globules are glassy is important for the electron microprobe analyses. The analyses have been done with a focused beam to avoid hitting the small chromites as much as possible. Under these conditions, large fractions of sodium can be lost from glass, which would explain the low totals. Correcting the Na concentrations to make totals equal 100 bring them into the range of 10–19 wt% Na_2O (mean

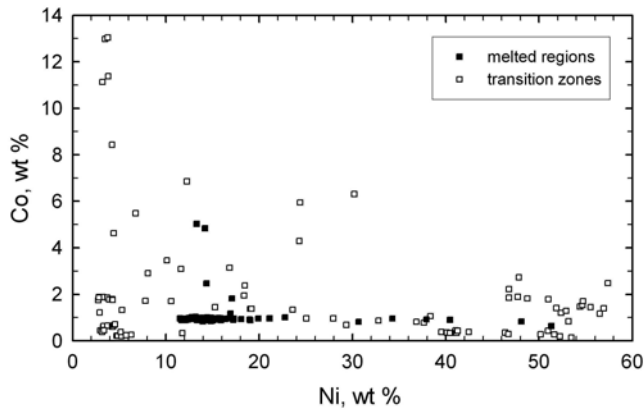


Fig. 5. Co content as a function of Ni content in metal grains. Solid squares = melted regions; open squares = transition zones. Five points with Co content larger than 1 wt% are from two metal cells in a melted region. Other points with Co content >2 wt% and Ni content <31 wt% are from six grains in one transition zone (not associated with the latter melted region).

14.1 wt%), leaving the average composition of the phosphates still slightly Na-poor and Fe-rich compared to maricite.

Transition Zones

The transition zones between the melted regions and the host chondrite have a chondritic texture, with no evidence of shock-melting of silicates. They vary in width from 0.1 to 2 mm. Melted metal forms globules and metal-troilite associations. Its Ni content is similar to that of metal in the melted regions, but it has much lower concentrations of phosphorus (Table 3; Fig. 6). Many of the metal particles have not been melted. Their Ni contents are in agreement with those of kamacite and taenite (i.e., mostly tetrataenite) in the Krymka host. Overall, the Ni content of both melted and non-melted metal varies from 2.8 wt% to 57.4 wt%. The frequent detection of Cr in both kamacite and taenite (up to 0.5 wt%) results from numerous micro-inclusions of chromite, as in the host (Perron and Bourot-Denise 1992).

The wide variation of Co content (Fig. 5) is noteworthy. Out of 22 analyzed kamacite grains, 17 have Co content comprised within either 0.2–0.6 or 1.0–1.9 wt%, in rough agreement with that found in the host (Rambaldi and Wasson 1984), but in five grains much higher values were obtained (5.5, 8.4, 11.1, 11.4, and 13.0 wt% Co, respectively). Some of these Co-rich grains are associated with a higher-Ni phase, which is also Co-rich, but less so than the kamacite itself (Co content in the ranges of 2.0–6.9 wt%). This is probably martensite, which indicates that these grains were partially melted, or at least were heated in part to the taenite stability field. Similarly, while six of the 14 tetrataenite grains analyzed (46.4–57.4 wt% Ni) have a Co content between 0.14 and 0.43 wt%, and one has a Co content of 0.84 wt%, the

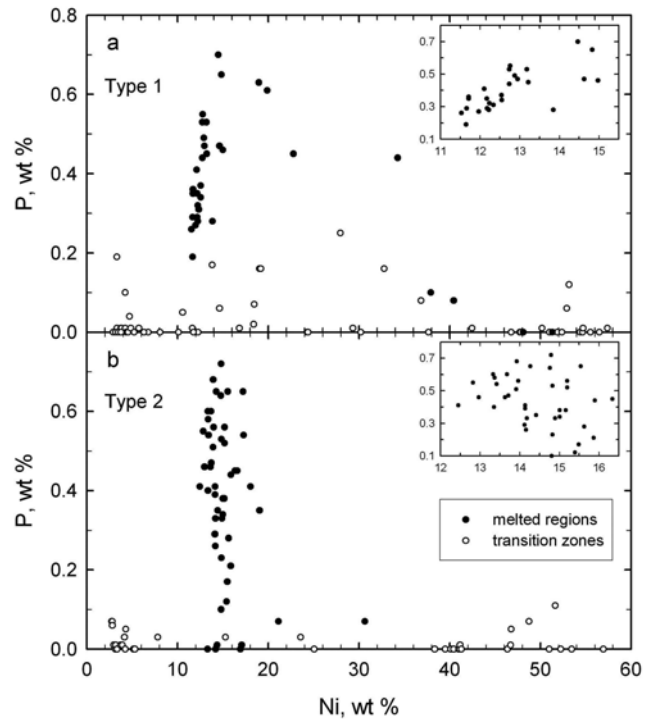


Fig. 6. P content as a function of Ni content in metal grains. a) type 1; b) type 2; solid circles, melted regions; open circles, transition zones. Insets show part of the same data on a different scale, to make clearer the presence or absence of a correlation between P and Ni contents.

other seven grains contain 1.2–2.5 wt% Co, which is a rather high range for tetrataenite. Some of these Co-rich tetrataenite grains are associated with the Co-rich kamacite. Intermediate Ni content values (23.6–42.5 wt%) may be ascribed in large part to analyses made near borders between kamacite or martensite and tetrataenite. This was found in 12 grains with Co content between 0.3 and 1.3 wt%, except for one grain with 4.3–6.3 wt% Co, associated with Co-rich kamacite and tetrataenite. The troilite has been completely melted and forms a dense network of veins and globules, in addition to associations with metal. Its composition range is the same as that of troilite in the melted regions (Table 3), except for one point at 9.2 wt% Ni, probably due to a small area of an Ni-rich sulfide, perhaps pentlandite.

DISCUSSION

As a whole, the light-colored melted regions described above are similar to impact melt-rock clasts found in many chondrites (Rubin 1985 and references therein). Their igneous, porphyritic, or skeletal texture, which implies local total or near-total melting, has been already observed in a number of clasts. However, they also have more specific characteristics, which we will emphasize below.

The presence of a partially melted transition zone between the melted regions and the host is unusual for melt-

Table 3. Electron microprobe analyses (wt%) of metal and troilite in Krymka transition zones.^{a,b}

	Kamacite (37)		Martensite (13)		Intermediate Ni (19)		Tetrataenite (24)		Troilite (19)	
	range	mean	range	mean	range	mean	range	mean	range	mean
Fe	82.9–97.5	93.3	78.3–87.6	82.7	55.1–74.3	63.2	39.3–53.0	46.6	54.1–63.2	60.7
Ni	2.75–8.07	4.27	10.1–19.2	14.8	23.6–42.5	34.6	46.4–57.4	51.7	n.d. ^c –9.18	1.39 ^d
Co	0.20–13.1	2.66	0.33–6.86	2.24	0.34–6.31	1.43	0.14–2.73	1.26	0.06–0.34	0.14
Cu	n.d.–0.06	<0.05	n.d.	<0.05	n.d.–0.21	0.09	n.d.–0.23	0.08	n.d.–0.13	<0.05
Cr	n.d.–0.39	0.07	n.d.–0.09	<0.02	n.d.–0.06	<0.02	n.d.–0.51	0.06	n.d.–0.06	<0.02
P	n.d.–0.19	<0.02	n.d.–0.17	0.06	n.d.–0.25	0.03	n.d.–0.12	<0.02	n.d.–0.11	<0.02
S	n.d.–0.27	0.05	n.d.–0.23	0.09	n.d.–0.81	0.15	n.d.–0.36	0.04	37.0–39.4	38.1
Total		100.5		99.9		99.6		99.8		100.5

^aThe number of analyses is given in parentheses.

^bThe separation between the different kinds of metal is somewhat arbitrary and essentially based on Ni content.

^cn.d. = not detected; the detection limits are given in the “mean” columns, when applicable.

^d0.96 when not taking into account the highest Ni content value.

rock clasts and indicates that shock melting occurred in situ. In contrast to most melt-rock clasts described previously (Rubin 1985), melting was not accompanied by total loss of metal and sulfide, which also points to in situ closed system melting. Following the usual nomenclature (Rubin 1985; Stöffler et al. 1991), these melted regions should thus be considered large melt pockets. According to Stöffler et al. (1991), whole rock melting requires shock pressures on an order of 75–90 GPa in non-porous chondritic matter, but could start at 30–35 GPa in porous material. The melted regions in Krymka may thus have formed at relatively low shock pressure, thanks to the presence of porous, volatile-rich, fine-grained matrix in type 3 material. Total melting means that the temperature in the melted regions rose above ~1500° C (calculated after Herzberg 1979). However, the materials in these regions remained melted only for a very short time, since chemical homogenization of the silicate melt did not take place, as shown by the chemical heterogeneity of olivines and mesostasis. Indeed, although the Fa content distribution in olivine is narrower than in the host (Fig. 2), it is still far from equilibration.

Cooling Rates at High Temperatures

Many of the chemical and mineralogical features we observed, such as the zoned composition of olivine, metal, and chromite, the presence of a cryptocrystalline mesostasis, the skeletal morphology of olivine and pyroxene, and the presence of P in metal and of Ni in troilite, indicate non-equilibrium crystallization conditions resulting from a high cooling rate. Experimental data on Fa zoning in olivine (Radomsky and Hewins 1990), Ni content in troilite (Smith and Goldstein 1977), and structural features of iron-nickel in metal-sulfide grains (Scott 1982) allow us to estimate the rate.

Most olivine crystals are normally zoned. According to experimental data, the degree of Fe-Mg zoning in olivine increases with FeO content and with cooling rate (Bianco and Taylor 1977; Radomsky and Hewins 1990). Fa-CaO zoning trends of the olivine crystals in the melted regions (5–

10 mol% Fa variation from core to edge) are very similar to those of crystals in Krymka type II porphyritic olivine chondrules and also to artificial crystals cooled at a rate of 1000 °C/h (Radomsky and Hewins 1990; see Fig. 3).

Most of the analyzed troilites contain measurable amounts of nickel. The average Ni-concentration in troilite is similar in the melted regions and the transition zones (1.10 and 0.97 wt%, respectively). Smith and Goldstein (1977) showed that the higher the cooling rate is, the higher the Ni concentration in troilite is. From their data, one can deduce that troilite in the melted regions cooled faster than 100 °C/h, and perhaps much faster than that.

The structure of the studied metal-troilite mixtures is coarser than those commonly observed in black veins of ordinary chondrites (Semenenko and Golovko 1994), but finer than those of fast-solidified grains from various chondrites studied by Scott (1982). The cooling rate R of metal of melted regions in the interval 1350–950 °C is estimated at ~300 °C/s using the equation $R = 530000d^{-2.9}$, where d is the spacing (in μm) between secondary metal dendrite arms or the width of elongated metal cells (Scott 1982). This calculated cooling rate is at least two orders of magnitude higher than that indicated by olivine zoning, taking into account the uncertainty of a factor of 12–15 estimated by Scott (1982). It can be noted that the dendrite spacing method led to cooling rates of 400 and 100 °C/h for the chondrites Ramsdorf and Rose City, respectively, (Scott 1982) while Smith and Goldstein (1977), from a study of metal-troilite intergrowths and including Ni content in troilite, estimated cooling rates of 100 °C/day and 1 °C/a for the same chondrites. Lacking a more precise assessment, it seems safe to state that the melted regions cooled faster than 100 °C/h, and possibly much faster.

Composition of the Opaque Phases

Zoned composition and presence of P are distinguishing features of metal in the melted regions. According to Begemann and Wlotzka (1969) the Ni-rich rim around metal

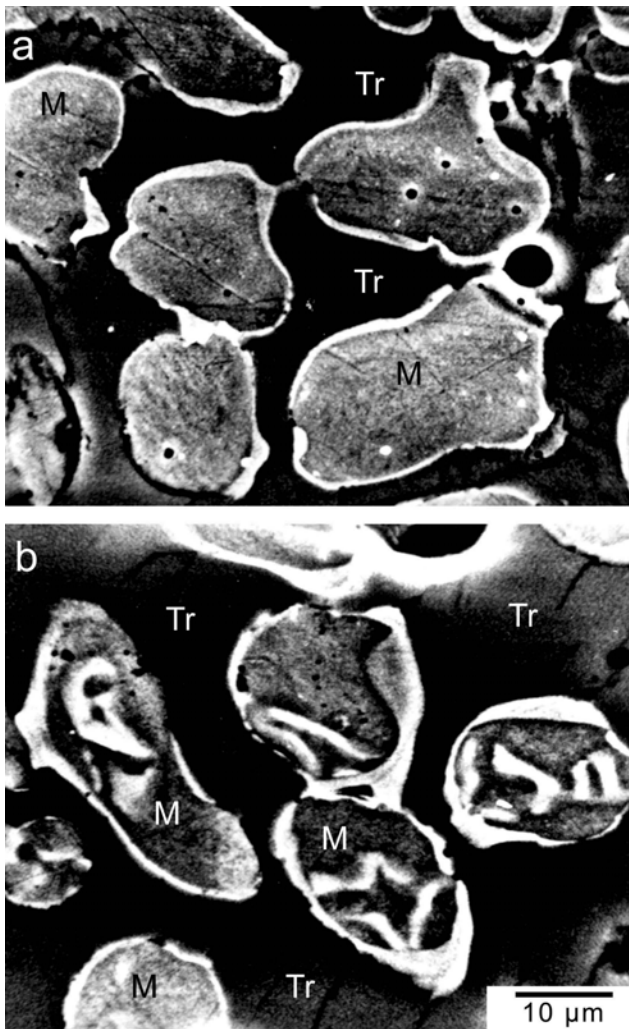


Fig. 7. Secondary electron images of metal (M)-troilite (Tr) intergrowths after etching with 5%-nital. a) type 1; b) type 2. Black spots in metal are holes probably left by phosphides. Metal cells of both types have Ni-enriched rims, but only type 2 metal also contain ribbon-like Ni-rich zones within the cells. Scale bar is 10 μm for both photos.

cells in troilite is caused by the fast crystallization of Fe-Ni from the Fe-Ni-S melt, which leads to Ni enrichment of the residual liquid. The Ni enrichment of the liquid must further increase when FeS starts to solidify. The tiny Ni-rich metal cells found in troilite certainly also result from late crystallization from the Ni-rich liquid.

The presence of P in shock-melted chondritic metal is common and is attributed to the reduction of phosphates at high temperature followed by dissolution of phosphorus in the liquid metal (Taylor and Heymann 1971; Smith and Goldstein 1977). This explanation is all the more valid here since in the Krymka host, as in other type 3 ordinary chondrites, P is associated with opaques, occurring as small Ca phosphates in cracks and at grain boundaries in troilite and metal grains (Rubin and Grossman 1985), and, more rarely, as

microscopic Fe phosphate inclusions in metal (Perron and Bourot-Denise 1992). This is also true for chromium, which is present in a large proportion of metal grains in the Krymka host as μm -size chromite inclusions (Perron and Bourot-Denise 1992). In the melted regions P and Cr, originally in phosphate and chromite, were reduced at high temperature and dissolved in the Fe-Ni-S melt. This fast reduction was favored by the small sizes of the phosphate and chromite crystals, and perhaps also by the presence of carbon, a possible reducing agent, in the matrix. Upon cooling, P partitioned between the solidifying metal and the S-rich melt, while Cr remained nearly entirely in the melt, as attested to by the near-total absence of Cr in the metal cells. This conforms with the chalcophile character of chromium in metal-troilite melts (Drake et al. 1978). As Fe-Ni crystallization proceeded, the Ni-enriched liquid became enriched in P as well, which produced the P-Ni correlation observed in the metal. Such a correlation is known for iron meteorites on a much larger scale (e.g., Haack and Scott 1993).

Upon further cooling, T-fO₂ conditions favoring the oxides were reached again and Cr and P were re-oxidized, yielding crystals of chromite and droplets of a phosphate-rich liquid immiscible with the Fe-Ni-S melt. Some chromium was incorporated in these droplets, precipitating as μm -size chromites, probably before solidification of the phosphate. The fast oxidation of P in the liquid suppressed its incorporation into the crystallizing metal, which explains the breakdown of the P-Ni correlation for larger values of Ni content. This correlation apparently stops in the type 2 metal at lower values of Ni content than in the type 1 metal, judging from the low statistics above 13.5 wt% Ni in type 1 (Fig. 6). Total re-oxidation in the melt was achieved before complete solidification of metal and troilite, as the Ni-rich rim around metal cells and the tiny Ni-rich cells, which represents the last metal to crystallize, are devoid or nearly devoid of P. Again, it seems that the P content falls to zero faster in type 2 than in type 1 metal. These differences may be due to a higher local oxygen fugacity in type 2 regions, which allowed oxidation of P at higher temperatures. This is consistent with the larger size of the phosphate globules and the apparently higher Fe₂O₃ content of the chromites in type 2 regions.

Cooling was too fast for P to be oxidized within the solid metal; tiny schreibersites precipitated instead, with some P remaining in the (metastable) solid solution. Cooling was also too fast for martensite to decompose, at least on the scale relevant to our means of observation. Experiments by Romig and Goldstein (1981) show that the appropriate conditions exist for precipitation of schreibersite without decomposition of martensite. The schreibersite inclusions may contribute to the observed P-Ni correlation, but they appear to be too few to explain it alone (Fig. 7). Moreover, the respective variation ranges of P and Ni contents do not correspond to what would be expected from a contribution from schreibersite.

We have no satisfactory explanation for the Ni-rich ribbons in the metal of type 2. They might be the result of martensite decomposition, but the rather high Ni content outside these ribbons, which are about as high as or higher than in type 1 martensite, does not support this hypothesis.

Quenching of the phosphate liquid resulted in the glassy globules in the troilite. The composition of these phosphate globules is unusual, being Na-rich and devoid of Ca. Phosphate globules rich in sodium have been observed in melted troilite in the heavily shocked H6 chondrite Yanzhuang (Chen and Xie 1996), although much less so than those of Krymka; tiny maricite (FeNaPO_4) crystals have been found in metal-troilite grains in Bishunpur (Mostefaoui 1996; Lauretta et al. 2001). Sodium is volatile and can be readily vaporized during shock heating of chondritic material. In addition, it has been shown experimentally that in Fe-S-silicate melts, alkalis (Na, K) partition in a significant proportion into the Fe-S liquid (Gessmann and Wood 2002; Murthy et al. 2003), which can also accommodate large amounts of oxygen (Gessmann and Wood 2002). These experiments were done at high pressures, but the effect of pressure was found to be nil between 1 and 3 GPa (Murthy et al. 2003) or weak between 2.5 and 24 GPa (Gessmann and Wood 2002), with the Fe-S/silicate partition coefficient increasing with decreasing pressure. In any case, these pressure ranges may not be irrelevant to shock melts. It thus seems highly likely that Na, vaporized in Krymka melted regions, dissolved in part in the Fe-Ni-S melt, along with some K and Mn. Reaction with dissolved P and O then led to the formation of the phosphate globules. Some of these globules also contain various amounts of Si, Mg, and Ca. This may be due to small silicate fragments or droplets trapped in the Fe-Ni-S melt that could have served as seeds for nucleation of the phosphates.

Shear deformations in phosphate globules (and also some grains of troilite) were caused by at least one additional shock, which occurred after solidification of the shock melts and had, in this part of Krymka, much weaker effects.

Comparison with Chondrules

The time-temperature conditions experienced by the shock-melted material in Krymka are qualitatively similar to those of chondrule formation: short heating to high temperatures, followed by fast cooling, which led to similar overall silicate texture and zoning. Although the starting materials were probably different, it may be interesting to compare in some detail the results of the two processes, in particular for the opaque phases.

In both the Krymka melted regions and the unmetamorphosed or little metamorphosed type I chondrules as found in type 2 carbonaceous chondrites (Grossman and Olsen 1974; Weisberg et al. 1993) and also in the LL3.0 ordinary chondrite Semarkona (Zanda et al. 1994), P and Cr

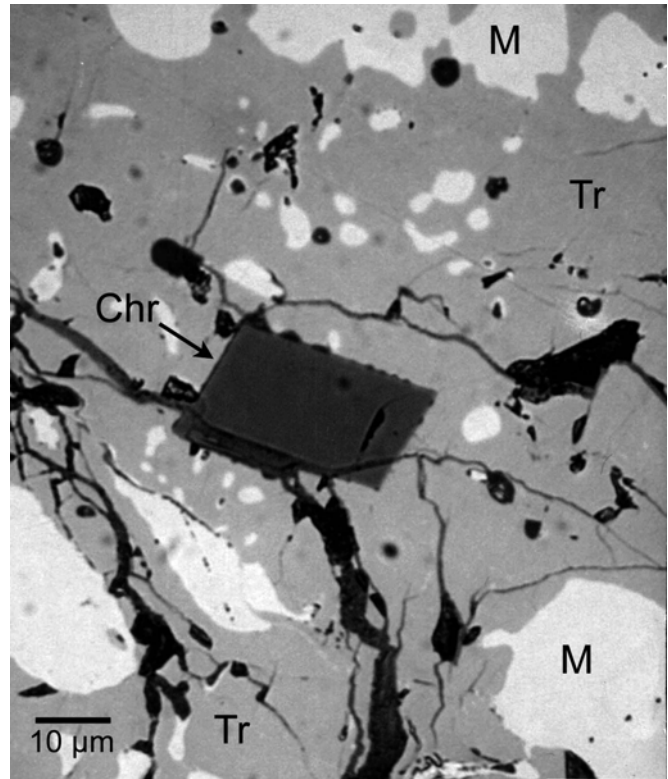


Fig. 8. Reflected light photomicrograph of a euhedral chromite crystal (Chr), set within a metal (M)-troilite (Tr) intergrowth of the first type. Dark veins contain iron hydroxides resulting from terrestrial oxidation. Scale bar is 10 μm .

are in a large part associated with metal or troilite. However, the associations are somewhat different in these two kinds of objects. In Krymka melted regions, as described above, P is found mostly dissolved in Fe-Ni and in oxidized form in troilite. Cr is present only in troilite, in oxidized form. In primitive type I chondrules, where primary troilite is generally rare, both P and Cr are dissolved in metal. The rarity of sulfide in these chondrules is likely due to its volatilization during chondrule melting (Yu et al. 1996). On the contrary, the Krymka melted regions, surrounded by cold, solid matter, apparently behaved as closed systems and, at least in large part, kept their troilite in intergrowths with Fe-Ni.

The fact that P and Cr are in oxidized form in the troilite of melted regions may reflect a higher oxygen fugacity than in type I chondrules, as attested by the higher FeO content of the silicates. Alternatively, it may be due to the lower solidification temperature of troilite compared to metal. At a given $f\text{O}_2$, lowering the temperature favors the formation of the oxides. Cr and P in troilite could reach lower temperatures while troilite was still liquid, allowing much faster diffusion than in solid metal, and thus making oxidation and precipitation feasible. P in metal is still in reduced form, as in primitive chondrule metal.

The Na-Fe phosphate globules found in the troilite of the melted regions are unknown in chondrules. They certainly

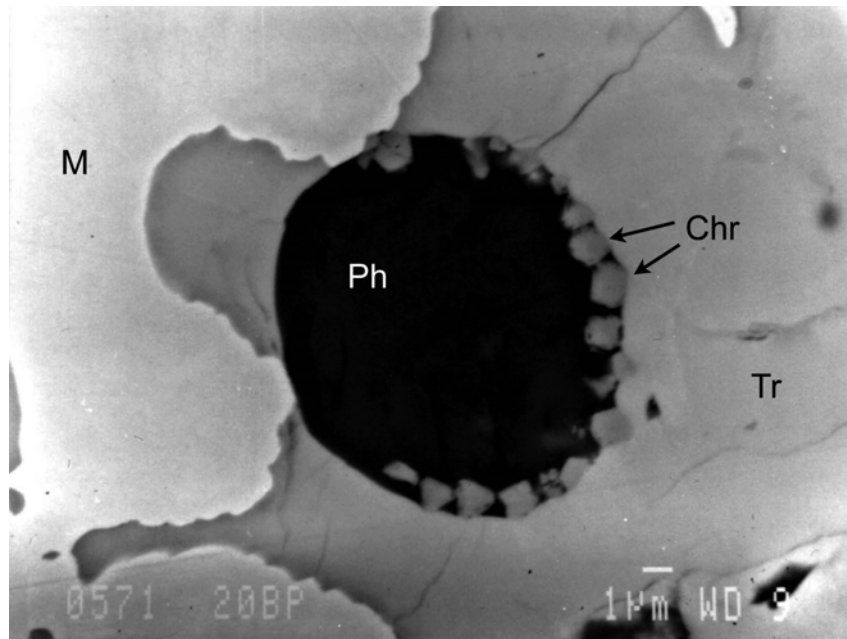


Fig. 9. A BSE image of a phosphate globule (Ph) with euhedral chromite microcrystals (Chr) within an intergrowth of metal (M) and troilite (Tr) of the second type. Scale bar is 1 μm .

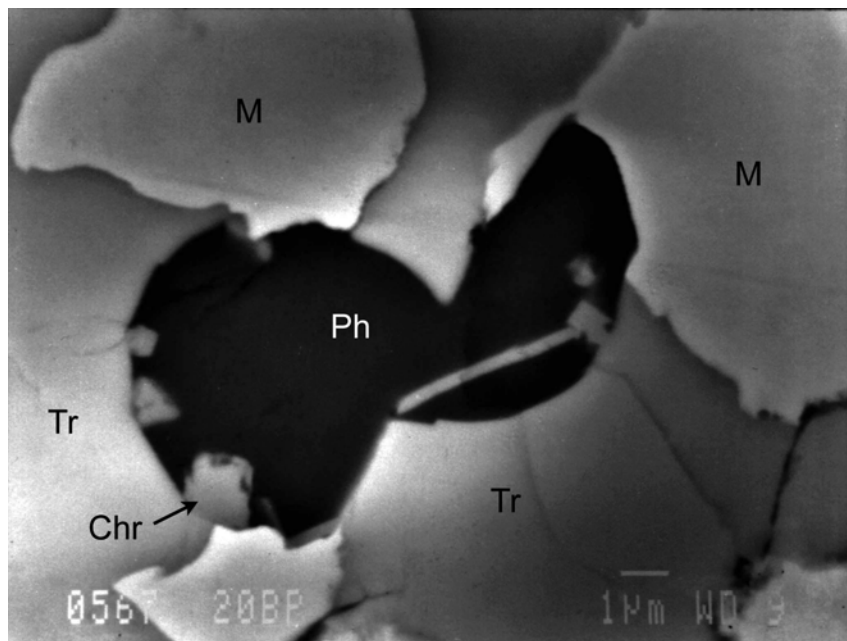


Fig. 10. A BSE image of a phosphate globule (Ph) with evidence of shear deformation. This structural feature demonstrates that at least one additional shock occurred after solidification of the phosphate. M = metal; Tr = troilite; Chr = chromite. Scale bar is 1 μm .

result from redistribution of sodium during melting. In chondrules, too, sodium can be mobilized, which leads in some chondrules to important sodium loss (Sears et al. 1996). Again, the closed system behavior of the melted regions prevented the escape of a large fraction of sodium, while the presence of abundant troilite probably helped incorporation of Na in the molten metal (Chabot and Drake 1999).

Finally, it is worth recalling that, while in the melted regions the metal is P-rich but devoid of Cr, Krymka host metal rarely contains P but is frequently Cr-rich (Rambaldi and Wasson 1984; Perron and Bourot-Denise 1992). Thus, the composition of the metal after the heating event does not directly reflect its initial composition. This should also be true for chondrules and supports the view that metal composition

in primitive chondrites is primarily due to the chemical processes that took place during chondrule melting, not due to the composition of the metal in the precursors (Zanda et al. 1994).

High-Co Metal Grains

A noticeable feature of our analyses is the high Co contents found in the metal of a transition zone, and, to a lesser extent, of a melted region (not associated with each other). High-Co, low-Ni metal grains (up to 39 wt% Co) have been found in equilibrated LL chondrites (Afiattalab and Wasson 1980; Rubin 1990). Such occurrences have also been observed in a few unequilibrated chondrites: in Colony CO3 (Rubin et al. 1985), in two xenoliths in Leoville CV3 (Kracher et al. 1985), in the ungrouped carbonaceous chondrite Ningqiang (Hua et al. 1995), and in Y-74660 LL3.0 (Kimura 2000). In Krymka, many analyses of metal grains in different samples did not bring in Co content values higher than 2 wt% in kamacite and 1.5 wt% in tetrataenite (Rambaldi and Wasson 1984; Perron and Bourot-Denise 1992 and unpublished), except for one kamacite grain and one tetrataenite grain with 2.7 and 2 wt% Co, respectively (Semenenko et al. 1987). Thus, the high values of Co content and the relative abundance of Co-rich grains in our samples seem to be a local peculiarity. This, together with the fact that the Co-rich grains are in zones strongly affected by shock, leads us to think that the Co enrichment is a shock effect.

The mechanism by which such an enrichment can occur could be removal of Fe in metal grains by chemical reactions, increasing the bulk Ni and Co contents in the residual metal. This would lead to a larger taenite fraction, and a larger Co content in kamacite (and also in taenite). This view is supported by the observation of Co-rich tetrataenite and its association with some of the Co-rich kamacite grains. The most likely reaction appears to be sulfurization by sulfur vapor formed in the melted regions. There is indeed evidence for sulfur vaporization when chondrites are shock melted (Rubin 2002). A limited amount of sulfur may have been vaporized in the melted regions and the vapor may have reacted with metal grains.

The two Co-rich cells found in one melted region, 15 μm distant from each other, are the only ones devoid of phosphorus out of 64 metal cells analyzed in melted regions. This strongly suggests that they are unmelted relics of a large grain. If this is the case, it seems plausible that their cobalt enrichment results from corrosion by sulfur vapor, as they were then the only (or maybe two of the rare) solid pieces of metal present in the melted regions at high temperatures.

Raising the Co content of the residual kamacite to 5.5–13 wt% as observed in a transition zone requires that a large fraction of the original metal be sulfurized, which would leave Co-rich grains associated with much larger amounts of troilite. This is not what is observed in the transition zone, as the Co-

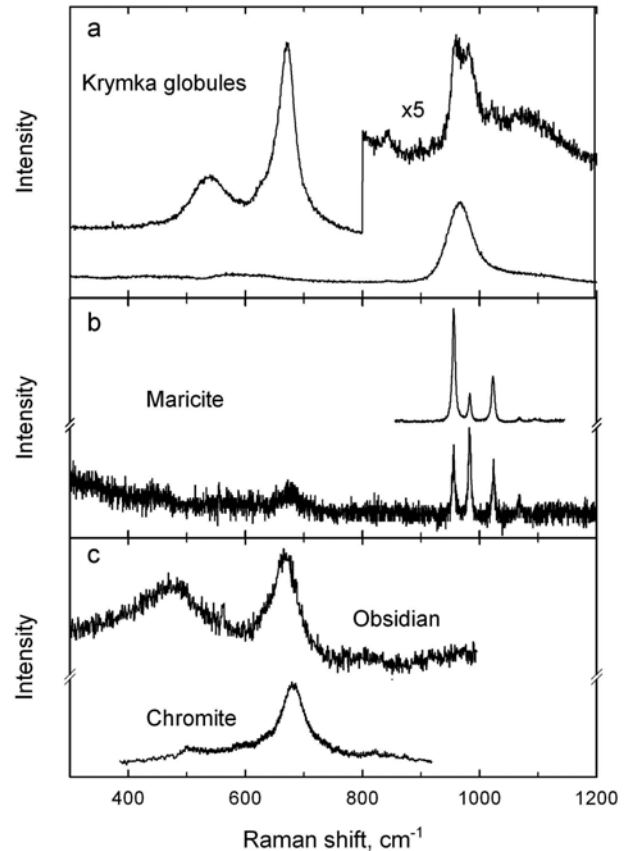


Fig. 11. Raman spectra of a) two globules included in troilite in Krymka melted regions, b) two maricite inclusions in the metal of the Bishunpur chondrite, c) a sample of obsidian (from Montagnac 2004) and a chromite inclusion in the metal of the Forest Vale chondrite.

rich grains are associated with little troilite. However, as all troilite in the transition zones appears to have been melted, troilite resulting from sulfurization of metal may have melted and flowed away through cracks and voids as soon as it formed. As this is not firmly established, we cannot entirely reject the possibility that the transition zone Co-rich grains already existed before the shock, but we do not favor this hypothesis by analogy with the Co-rich cells of the melted region.

It should be noted that the graphite-rich xenoliths studied by Semenenko et al. (2004), which come from the same hand specimen as the melted regions reported here, also contain Co-rich metal. However, the Co content of the latter does not exceed 3.2 wt%, and it seems improbable that any genetic relationship exists between these two sorts of objects.

CONCLUSION

The Krymka individual specimen #1290/29 of the Kyiv collection shows stronger shock effects than have been observed in the rest of the chondrite. In this specimen, millimeter- to centimeter-size regions have been completely

melted in situ and display an igneous texture. According to Stöffler et al. (1991), this implies a shock pressure in the range of 75–90 GPa in non-porous chondritic matter, but of only 30–35 GPa in porous material. Melting was very short, leaving no time for the silicate melt to chemically homogenize; cooling was faster than 100 °C/h at high temperature and possibly much faster. These time-temperature conditions are close to those of chondrule formation, and indeed some characteristics of the melted regions resemble those of unmetamorphosed chondrules, for example, silicate texture, olivine zoning, and the presence of P in metal. However, the particular setting of the melting process also led to features that are not observed in chondrules. Sulfur was not largely lost but a Fe-Ni-S melt formed large metal-troilite intergrowths. Cr partitioned into troilite rather than in metal and formed chromite crystals therein. The Fe-Ni-S melt also incorporated significant amounts of Na, which led to formation of a Fe-Na phosphate glass in troilite, with a composition close to that of maricite.

Highly Co-rich metal grains were found in one melted region and around another one. It is likely that they result from sulfurization of metal by sulfur vapor produced during the shock.

Mechanical deformations in the melted regions are evidence that at least one other shock occurred after they solidified.

The Krymka specimen we have studied has suffered somewhat extreme shock metamorphism and may not be representative of the bulk of the meteorite. However, one should keep in mind that strong shock effects do exist in Krymka, especially when dealing with the primitive properties of this seemingly very little metamorphosed chondrite.

Acknowledgments—We thank J. Barandon, P. Blanc, C. Fiéni, A. Girich, G. Montagnac, G. Sagon and V. Sobolev for help with the various instruments used. We also thank reviewers M. Kimura and A. Rubin for constructive comments on the manuscript. This work was supported in part by INTAS and by INSU-CNRS Programme National de Planétologie.

Editorial Handling—Dr. Ed Scott

REFERENCES

- Afiattalab F. and Wasson J. T. 1980. Composition of the metal phases in ordinary chondrites: Implications regarding classification and metamorphism. *Geochimica et Cosmochimica Acta* 44:431–446.
- Begemann F. and Wlotzka F. 1969. Shock induced thermal metamorphism and mechanical deformations in the Ramsdorf chondrite. *Geochimica et Cosmochimica Acta* 33:1351–1370.
- Bianco A. S. and Taylor L. A. 1977. Application of dynamic crystallization studies: Lunar olivine normative basalts. 8th Lunar and Planetary Science Conference, pp. 1593–1610.
- Bunch T. E., Keil K., and Snetsinger K. G. 1967. Chromite composition in relation to chemistry and texture of ordinary chondrites. *Geochimica et Cosmochimica Acta* 31:1569–1582.
- Chabot N. L. and Drake M. J. 1999. Potassium solubility in metal: The effects of composition at 15 kbar and 1900 °C on partitioning between iron alloys and silicate melts. *Earth and Planetary Science Letters* 172:323–335.
- Chen M. and Xie X. D. 1996. Na behaviour in shock-induced melt phase of the Yanzhuang (H6) chondrite. *European Journal of Mineralogy* 8:325–333.
- Dodd R. T., Van Schmus W. R., and Koffman D. M. 1967. A survey of the unequilibrated ordinary chondrites. *Geochimica et Cosmochimica Acta* 31:921–951.
- Drake M. J., Bild R. W., and Hostetler C. J. 1978. Experimental investigations of trace element fractionation in iron meteorites. I. Preliminary results for Cr (abstract). 9th Lunar and Planetary Science Conference, pp. 264–266.
- Gessmann C. K. and Wood B. J. 2002. Potassium in the Earth's core? *Earth and Planetary Science Letters* 200:63–78.
- Grossman L. and Olsen E. 1974. Origin of the high-temperature fraction of C2 chondrites. *Geochimica et Cosmochimica Acta* 38:173–187.
- Haack H. and Scott E. R. D. 1993. Chemical fractionation in Group IIIAB iron meteorites: Origin by dendritic crystallization of an asteroidal core. *Geochimica et Cosmochimica Acta* 57:3457–3472.
- Herzberg C. T. 1979. The solubility of olivine in basaltic liquids: An ionic model. *Geochimica et Cosmochimica Acta* 43:1241–1251.
- Hua X., Eisenhour D. D., and Buseck P. R. 1995. Cobalt-rich, nickel-poor metal (wairauite) in the Ningqiang carbonaceous chondrite. *Meteoritics* 30:106–109.
- Kimura M. 2000. Opaque minerals in an LL3.0 chondrite, Y-74660: Potential indicators of petrologic subtypes (abstract #1213). 31st Lunar and Planetary Science Conference. CD-ROM.
- Kracher A., Keil K., Kallemeyn, G. W., Wasson J. T., Clayton R. N., and Huss G. I. 1985. The Leoville (CV3) accretionary breccia. 16th Lunar and Planetary Science Conference, *Journal of Geophysical Research* 90:D123–D135.
- Lauretta D. S., Buseck P. R., and Zega T. J. 2001. Opaque minerals in the matrix of the Bishunpur (LL3.1) chondrite: Constraints on the chondrule formation environment. *Geochimica et Cosmochimica Acta* 65:1337–1353.
- Montagnac G. 2004. Handbook of Raman spectra of minerals. <http://www.ens-lyon.fr/LST/Raman>. Last accessed on February 15, 2005.
- Mostefaoui S. 1996. Metal and carbon in primitive ordinary chondrites: Physico-chemical implications for the early solar system. Ph.D. thesis, Muséum National d'Histoire Naturelle, Paris.
- Murthy V. R., Van Westrenen W., and Fei Y. 2003. Experimental evidence that potassium is a substantial radioactive heat source in planetary cores. *Nature* 423:163–165.
- Perron C. and Bourot-Denise M. 1992. Inclusions in the metal of Tieschitz and Krymka (abstract). 23rd Lunar and Planetary Science Conference, pp. 1055–1056.
- Radomsky P. M. and Hewins R. H. 1990. Formation conditions of pyroxene-olivine and magnesian olivine chondrules. *Geochimica et Cosmochimica Acta* 54:3475–3490.
- Rambaldi E. R. and Wasson J. T. 1984. Metal and associated phases in Krymka and Chainpur: Nebular formation processes. *Geochimica et Cosmochimica Acta* 48:1885–1897.
- Romig A. D. and Goldstein J. I. 1981. Low temperature phase equilibria in the Fe-Ni and Fe-Ni-P systems: Application to the thermal history of metallic phases in meteorites. *Geochimica et Cosmochimica Acta* 45:1187–1197.
- Rubin A. E. 1985. Impact melt products of chondritic material. *Reviews of Geophysics* 23:277–300.

- Rubin A. E. 1990. Kamacite and olivine in ordinary chondrites: Intergroup and intragroup relationships. *Geochimica et Cosmochimica Acta* 54:1217–1232.
- Rubin A. E. 2002. Smyer H-chondrite impact-melt breccia and evidence for sulfur vaporization. *Geochimica et Cosmochimica Acta* 66:699–711.
- Rubin A. E. and Grossman J. N. 1985. Phosphate-sulfide assemblages and Al/Ca ratios in type 3 chondrites. *Meteoritics* 20:479–489.
- Rubin A. E., James J. A., Keck B. D., Weeks K. S., Sears D. W. G., and Jarosewich E. 1985. The Colony meteorite and variations in CO₃ chondrite properties. *Meteoritics* 20:175–196.
- Scott E. R. D. 1982. Origin of rapidly solidified metal-troilite grains in chondrites and iron meteorites. *Geochimica et Cosmochimica Acta* 46:813–823.
- Sears D. W. G., Huang S., and Benoit P. H. 1996. Open-system behaviour during chondrule formation. In *Chondrules and the protoplanetary disk*, edited by Hewins R. H., Jones R. H., and Scott E. R. D. Cambridge: Cambridge University Press. pp. 221–231.
- Semenenko V. P. and Girich A. L. 1995. Mineralogy of a unique graphite-containing fragment in the Krymka chondrite (LL3). *Mineralogical Magazine* 59:443–454.
- Semenenko V. P. and Girich A. L. 1996. Graphite-containing fragments in the Krymka chondrite (abstract). *Meteoritics & Planetary Science* 31:A127.
- Semenenko V. P. and Girich A. L. 1998. The nature of graphite-containing fragments in the Krymka (LL3) chondrite (abstract). *Meteoritics & Planetary Science* 33:A141.
- Semenenko V. P. and Girich A. L. 2001. A variety of lithic fragments in the Krymka (LL3.1) chondrite (abstract). *Meteoritics & Planetary Science* 36:A187.
- Semenenko V. P. and Golovko N. V. 1994. Shock-induced black veins and organic compounds in ordinary chondrites. *Geochimica et Cosmochimica Acta* 58:1525–1535.
- Semenenko V. P. and Perron C. 1995. Shock-melted regions in the Krymka (LL3) chondrite (abstract). *Meteoritics* 30:577.
- Semenenko V. P. and Perron C. 1996. Shock-melted regions in the Krymka (LL3) chondrite. *Mineralogicheskii Zhurnal* 18:26–37. In Russian.
- Semenenko V. P., Sobotovich E. V., and Tertichnaya B. V. 1987. *Meteorites of Ukraine*. Kyiv: Naukova Dumka. 220 p. In Russian.
- Semenenko V. P., Bischoff A., Weber I., Perron C., and Girich A. L. 2001. Mineralogy of fine-grained material in the Krymka (LL3.1) chondrite. *Meteoritics & Planetary Science* 36:1067–1085.
- Semenenko V. P., Girich A. L., and Nittler L. R. 2004. An exotic kind of cosmic material: Graphite-containing xenoliths from the Krymka (LL3.1) chondrite. *Geochimica et Cosmochimica Acta* 68:455–475.
- Smith B. A. and Goldstein J. I. 1977. The metallic microstructures and thermal histories of severely reheated chondrites. *Geochimica et Cosmochimica Acta* 41:1061–1072.
- Stöffler D., Keil K., and Scott E. R. D. 1991. Shock metamorphism of ordinary chondrites. *Geochimica et Cosmochimica Acta* 55:3845–3867.
- Taylor G. J. and Heymann D. 1971. Postshock thermal histories of reheated chondrites. *Journal of Geophysical Research* 76:1879–1893.
- Weisberg M. K., Prinz M., Clayton R. N., and Mayeda T. K. 1993. The CR (Renazzo-type) carbonaceous chondrite group and its implications. *Geochimica et Cosmochimica Acta* 57:1567–1586.
- Yu Y., Hewins R. H., and Zanda B. 1996. Sodium and sulfur in chondrules: Heating time and cooling curves. In *Chondrules and the protoplanetary disk*, edited by Hewins R. H., Jones R. H., and Scott E. R. D. Cambridge: Cambridge University Press. pp. 213–219.
- Zanda B., Bourot-Denise M., Perron C., and Hewins R. H. 1994. Origin and metamorphic redistribution of silicon, chromium, and phosphorus in the metal of chondrites. *Science* 265:1846–1849.
-